Manifestations of multiple-carrier charge transport in the magnetostructurally ordered phase of $BaFe_2As_2$

S. Ishida,[1,2,3] T. Liang,[1,2,3] M. Nakajima,[1,2,3] K. Kihou,[2,3] C. H. Lee,[2,3] A. Iyo,[2,3] H. Eisaki,[2,3] T. Kakeshita,[1,3] T. Kida,[3,4] M. Hagiwara,[3,4] Y. Tomioka,[2,3] T. Ito,[2,3] and S. Uchida[1,3]

[1]*Department of Physics, University of Tokyo, Tokyo 113-0033, Japan*

[2]*National Institute of Advanced Industrial Science and Technology, Tsukuba 305-8568, Japan*

[3]*JST, Transformative Research-Project on Iron Pnictides, Tokyo 102-0075, Japan*

[4]*KYOKUGEN, Osaka University, 1-3 Machikaneyama, Toyonaka, Osaka 560-8531, Japan*

(Received 27 September 2011; revised manuscript received 20 October 2011; published 14 November 2011)

We investigated the transport properties of $BaFe_2As_2$ single crystals before and after annealing with BaAs powder. The annealing remarkably improves transport properties, in particular, the magnitude of residual resistivity, which decreases by a factor of more than 10. From the resistivity measurement on detwinned crystals, we found that the anisotropy of the in-plane resistivity is remarkably diminished after annealing, indicative of dominant contributions to the charge transport from the carriers with isotropic and high mobility below magnetostructural transition temperature T_s and the absence of nematic state above T_s. We found that the Hall resistivity shows strong nonlinearity against magnetic field, and the magnetoresistance becomes very large at low temperatures. These results give evidence for the manifestation of multiple carriers with distinct characters in the ordered phase below T_s. By analyzing the magnetic-field dependences, we found that at least three carriers equally contribute to the charge transport in the ordered phase, which is in good agreement with the results of recent quantum oscillation measurements.

DOI: 10.1103/PhysRevB.84.184514 PACS number(s): 74.70.Xa, 74.25.F−, 72.15.Gd, 75.47.−m

I. INTRODUCTION

Parent compounds of iron-based superconductors undergo a tetragonal-to-orthorhombic structural transition upon cooling accompanied by an antiferromagnetic (AFM) order and show anomalous metallic behavior.[1] In this ordered phase, spins align antiferromagnetically along the a axis and ferromagnetically along the b axis,[2] so the electronic state is essentially anisotropic. Recent in-plane resistivity measurements performed on detwinned crystals of $Ba(Fe_{1-x}Co_x)_2As_2$, $CaFe_2As_2$, and $SrFe_2As_2$ (Refs. 3–5) revealed an anomalous anisotropic electronic property that the resistivity along the AFM spin direction with longer lattice constant (a axis) is smaller than the resistivity along the ferromagnetic (FM) spin direction with shorter lattice constant (b axis), and this in-plane resistivity anisotropy can be seen in the tetragonal phase well above the phase transition temperature T_s, which has been discussed in terms of nematicity.[3] In relation to the nematicity, the orbital polarization above T_s is observed by angle-resolved photoemission spectroscopy (ARPES).[10] However, the in-plane resistivity above T_s is negligibly small in the cases of $CaFe_2As_2$ and $SrFe_2As_2$, which show a strongly first-order phase transition,[5] indicating that the in-plane resistivity anisotropy above T_s or nematicity might not be intrinsic, but could be induced by the external pressure.

The in-plane resistivity anisotropy of undoped $BaFe_2As_2$ is relatively small compared with underdoped $Ba(Fe_{1-x}Co_x)_2As_2$,[3] despite the fact that lattice orthorhombicity diminishes monotonically with increasing Co concentration.[6] The small anisotropy of undoped $BaFe_2As_2$ has been discussed from magnetotransport measurements in terms of a dominant role of isotropic and high-mobility Dirac pockets with the Dirac point near the Fermi energy E_F,[7,8] which were first observed by ARPES (the Dirac point is located at 1 ± 5 meV from E_F).[9] However, several Fermi-surface (FS) pockets other than Dirac pockets also exist in the ordered state as evidenced by ARPES (Refs. 10–12) and quantum oscillation.[13,14] In such a multiple-band system, is it really possible that such tiny Dirac pockets with very small density dominate the charge transport? Additionally, recent optical measurements performed on detwinned $BaFe_2As_2$ crystal[15] revealed that the almost isotropic Drude component existing along both the a and b axes dominates the dc conductivity. The estimated Drude weight is of the order of 10^{20} cm^{-3}, which seems too large to be formed only by tiny Dirac pockets. It seems that one needs another explanation for the small in-plane resistivity anisotropy of undoped $BaFe_2As_2$.

It is also reported that annealing remarkably improves transport properties in the ordered phase of $BaFe_2As_2$,[16] which indicates that the as-grown crystals contain an appreciable amount of defects and impurities, and hence the observation of the intrinsic charge transport in this system might be inhibited. Therefore, it is required to investigate the intrinsic transport properties of this compound using annealed crystals.

In this paper, we present the transport measurements on $BaFe_2As_2$ single crystals with much improved quality. We show that the in-plane resistivity anisotoropy both above and below T_s is diminished, and the in-plane resistivity becomes almost isotropic, which indicates that the nematicity may not be intrinsic. We also provide clear evidence from the magnetotransport measurements that multiple carriers contribute to the charge transport in the ordered phase of $BaFe_2As_2$. Only tiny Dirac pockets do not play a dominant role as previously reported, but contribution to the conductivity from at least three types of carriers mask the underlying anisotropic electronic states.

II. EXPERIMENTAL PROCEDURES

Single crystals of $BaFe_2As_2$ were grown by the self-flux method as described elsewhere.[17] The crystals were cut in a rectangular shape along the tetragonal [110] directions, which become a or b axes in the orthorhombic phase. Typical crystal dimensions were 1.5 × 1.5 × 0.5 mm^3, with the shortest edge along the c axis. Part of the crystals were sealed into an evacuated quartz tube together with Ba or BaAs powders and annealed for several days. A standard four-terminal method was used for the in-plane resistivity measurements on twinned crystals. The magnetoresistance (MR) and Hall resistivity ρ_{xy} were measured with the electrical current along the ab plane and the magnetic field along the c axis. For detwinning, the $BaFe_2As_2$ crystals were set into a uniaxial pressure cell and detwinned by applying compressive pressure along the tetragonal [110] direction.[18] The resistivity along the a and b axes was measured simultaneously using the Montgomery method[19] without releasing pressure. The measurements in the magnetic fields up to 7 T were performed in a Quantum Design physical property measurement system (PPMS). MR and ρ_{xy} in the magnetic fields up to 14 T were measured at the High Magnetic Field Laboratory, KYOKUGEN, Osaka University.

III. RESULTS AND DISCUSSION

A. Annealing effect on in-plane resistivity

Figure 1(a) shows temperature (T) dependence of the in-plane resistivity $\rho_{ab}(T)$ measured on twinned $BaFe_2As_2$ crystals annealed under various conditions. $\rho_{ab}(T)$ of the as-grown crystal (black dots) shows typical temperature dependence so far reported for this compound. $\rho_{ab}(T)$ drops at $T_s \sim$ 136 K, corresponding to the magnetostructural transition and

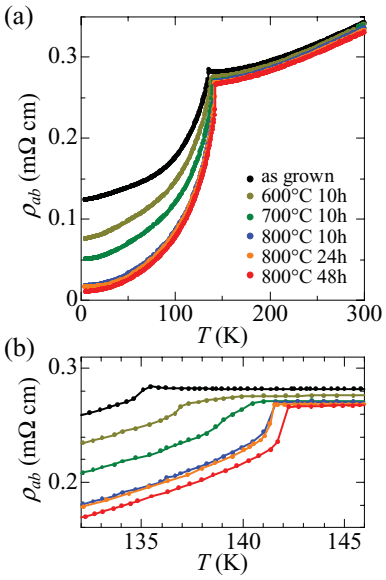

FIG. 1. (Color online) (a) Temperature dependence of the in-plane resistivity measured on twinned $BaFe_2As_2$ crystals before (as grown) and after annealing under various conditions shown in the figure. Single crystals were annealed together with BaAs. (b) Enlarged view of (a) around the magnetostructural transition temperature.

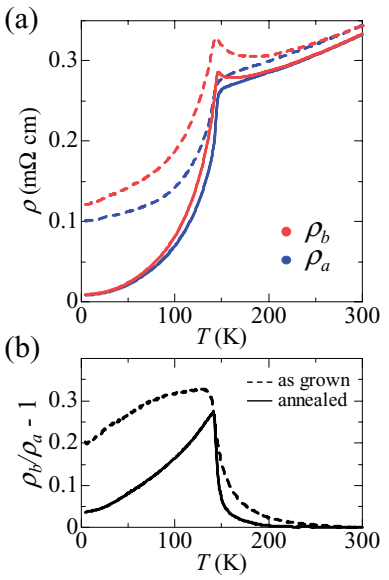

FIG. 2. (Color online) (a) Temperature dependence of the in-plane resistivity measured on detwinned $BaFe_2As_2$ crystals ρ_a (blue) and ρ_b (red). The dashed line and the solid line correspond to as-grown and annealed crystal, respectively. (b) Temperature dependence of anisotropy of the in-plane resistivity defined as ρ_b/ρ_a-1 for as-grown (dashed line) and annealed (solid line) crystals.

shows residual resistivity of typically 0.1 mΩcm. The residual resistivity ratio (RRR) defined as $\rho_{ab}(300\,K)/\rho_{ab}(5\,K)$ is about 3. Because the ordered state below T_s has orthorhombic crystal structure, the twinned crystal has domains with different orientations, hence, the scattering at domain boundaries could be a source of residual resistivity. However, this is unlikely as a main source of scattering in the present case since $\rho(T)$ of detwinned $BaFe_2As_2$ still shows large residual resistivity [see dashed curves in Fig. 2(a)].

The annealing remarkably reduced the residual resistivity in the ordered phase of $BaFe_2As_2$ as reported in Ref. 16. In general, the annealing process would remove crystal defects and lattice dislocations, which are possible scattering sources and can cause large residual resistivity. Rotundu *et al.* adopted low-pressure Ar gas annealing and obtained crystals with RRR ∼36 after 30-day annealing at 700 °C.[16] In order to shorten the annealing time, we annealed crystals in a evacuated quartz tube together with Ba or BaAs powders since we assumed that the main sources of scattering are defects and/or dislocations of Ba and/or As sites. However, annealing with Ba is found to not much improve the crystal quality since Ba reacts with crystals above 600 °C and RRR gets worse. We found that RRR can be improved more quickly by annealing with BaAs than Ar gas annealing. After annealing for 48 hours at 800 °C, we obtained crystal with RRR ∼34. However, it is still unclear why RRR of this compound is so sensitive to the annealing process.

Temperature dependence of $\rho_{ab}(T)$ for the annealed crystal seems almost unchanged above T_s after annealing, i.e., the annealing process scarcely affects the transport properties in the paramagnetic (PM) phase. On the other hand, as is shown in Fig. 1(b), T_s increases from 136 to 142 K, and

the phase transition becomes sharper probably because crystal defects are removed and it helps to stabilize the orthorhombic lattice and magnetic ordering. Remarkably, $\rho_{ab}(T)$ drops much steeper below T_s and goes down to ~10 $\mu\Omega$cm at $T = 5$ K, one order of magnitude smaller than the value of as-grown crystal. If the carrier density is unchanged after annealing as reported,[16] this indicates that carrier mobility is greatly enhanced by annealing.

B. In-plane resistivity anisotropy

The in-plane resistivities of detwinned $BaFe_2As_2$ crystal are shown in Fig. 2(a). Note that effects of annealing on the in-plane resistivity anisotropy are also discussed by Nakajima *et al.* in Ref. 15. The dashed line corresponds to resistivity components for the as-grown crystal. The blue and red colors correspond to resistivity along the a axis (ρ_a) and b axis (ρ_b), respectively. Around room temperatures, there is no appreciable difference between ρ_a and ρ_b. As temperature is lowered, ρ_a continues to decrease, while ρ_b shows an upturn toward T_s. The in-plane resistivity anisotropy can be seen well above T_s, from about 80 K above, and ρ_a is always smaller than ρ_b. These results reproduce the reported ones[3] and confirm that the crystal is successfully detwinned by our technique. The in-plane resistivity anisotropy defined as ρ_b/ρ_a-1 is plotted in Fig. 2(b). The anisotropy shows a maximum value ~0.33 just below T_s, but it is robust even at the lowest temperature (~0.2 at $T = 5$ K).

The solid lines in Fig. 2(a) show the resistivity components of the annealed crystal. The temperature dependence of ρ_a and ρ_b seems qualitatively similar to that of the as-grown crystal. However, the anisotropy becomes appreciable only about 40 K above T_s, that is, the phase transition becomes more first-order-like as seen in $SrFe_2As_2$ and $CaFe_2As_2$.[20,21] This suggests that the magnetostructural transition might essentially be of the first order even in the purest sample of $BaFe_2As_2$. Therefore, the in-plane resistivity anisotropy above T_s seems not originated from nematic phase but induced by the external pressure and/or remaining crystal defects and disorder. Remarkably, the anisotropy is much reduced as compared with that for as-grown crystal and diminishes as temperature is decreased below T_s, and the in-plane resistivity becomes nearly isotropic at temperatures well below T_s (ρ_b/ρ_a-1 ~ 0.04 at 5 K). In fact, the isotropic charge transport at low temperatures is consistent with the results of other experiments. ARPES (Refs. 10–12) and quantum oscillation[13,14] revealed ellipsoidal FS pockets, which, when summed over the momentum space, would result in isotropic conductivity. Also, the optical conductivity spectra of detwinned $BaFe_2As_2$ for light polarization along the a and b axes (measured crystals were annealed under the same condition)[15] are dominated by an isotropic Drude component with extremely high peak value (of the order of 10^5 Ω^{-1}cm^{-1} at $T = 5$ K) and narrow width, consistent with the dc resistivity. The anisotropy in optical conductivity shows up in the finite frequency region, which arises from anisotropic gap feature below T_s. The question is whether or not this Drude term originates from the tiny Dirac pockets. We will answer this after we show the results of magnetotransport measurements.

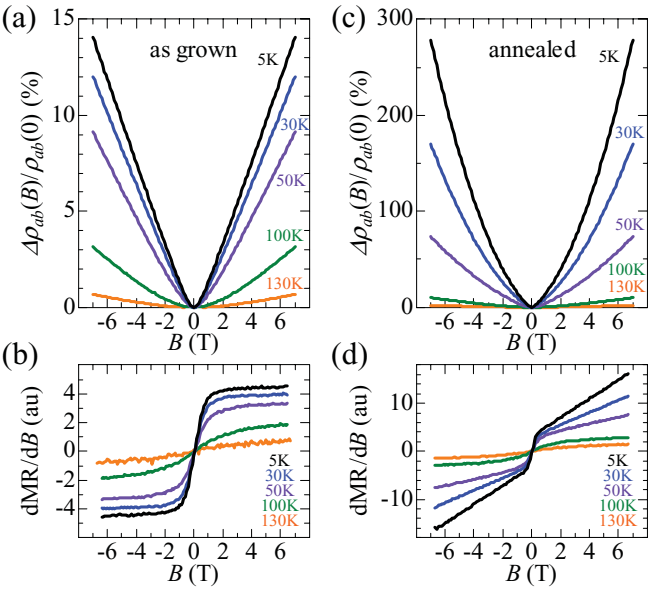

FIG. 3. (Color online) Magnetic-field dependence of the transverse magnetoresistnce [MR, $\Delta\rho_{ab}(B)/\rho_{ab}(B = 0)$] (a) and its field derivative (dMR/dB) (b) for the twinned as-grown $BaFe_2As_2$ crystal taken at several temperatures. (c), (d) Same plots for the annealed $BaFe_2As_2$ crystal.

C. Magnetoresistance

Figures 3(a)–3(d) show the magnetic-field (B) dependence of the magnetoresistance (MR) for transverse magnetic field ($B \parallel c$, $j \parallel ab$) and its derivative with respect to magnetic field for as-grown [Figs. 3(a) and 3(b)] and annealed [Figs. 3(c) and 3(d)] crystals, respectively. The magnitude of MR is defined as $\Delta\rho_{ab}(B)/\rho_{ab}(B = 0) = [\rho_{ab}(B) - \rho_{ab}(B = 0)]/\rho_{ab}(B = 0)$. In both cases, MR is smaller than 0.03% in the PM phase and rapidly increases below T_s. MR of the as-grown crystal is 14% at $B = 7$ T and $T = 5$ K [Fig. 3(a)] and shows almost B linear dependence above 1 T, which is more clearly seen in the B dependence of the derivative of MR (dMR/dB) [Fig. 3(b)]. B linear MR is anomalous since, in the framework of a simple two-carrier model, MR at low fields can be written in the form of $(\mu_M B)^2$, where μ_M is magnetoresistance mobility, and MR saturates at high fields where $\mu_M B$ or $\omega_c\tau > 1$. Huynh *et al.* ascribed this nonsaturating linear MR to a quantum transport of Dirac-cone states[7] based on a model proposed by Abrikosov.[22] However, recent study of MR for as-grown $BaFe_2As_2$ under higher magnetic field up to 50 T showed nonlinear but quadratic B dependence of MR at high fields,[23] revealing the complicated B dependence of MR.

In the case of the annealed crystal, MR reaches ~280% at $B = 7$ T and $T = 5$ K [Fig. 3(c)], which is by an order of magnitude larger than that of the as-grown crystal. Furthermore, in contrast to the case of the as-grown crystal, MR shows quadratic B dependence up to 7 T. Considering that the magnitude of MR is a measure of carrier mobility, the mobility of carriers should be greatly enhanced by the annealing, which is consistent with the decrease of residual resistivity. Note that dMR/dB has a kinklike structure at low field around 0.5 T, that is, MR of annealed crystal also has some B linear component similar to the case of the as-grown crystal

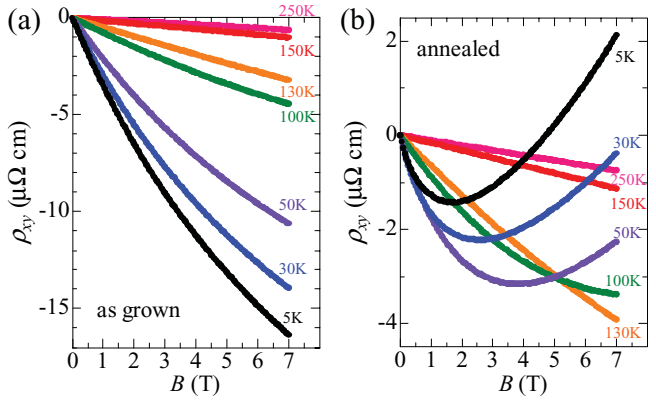

FIG. 4. (Color online) Magnetic-field dependence of the Hall resistivity ρ_{xy} of twinned as-grown (a) and annealed (b) $BaFe_2As_2$ crystals taken at several temperatures.

[Fig. 3(d)], suggestive of a contribution from Dirac pockets. However, observed large and quadratic B-dependent MR gives evidence that other FS pockets have appreciable contribution to the charge transport in the ordered phase of $BaFe_2As_2$.

D. Hall effect

Figure 4(a) shows the magnetic-field dependence of the Hall resistivity ρ_{xy} ($B \parallel c$, $j \parallel ab$) for the as-grown crystal taken at several temperatures. $\rho_{xy}(B)$ of the as-grown crystal shows basically B linear dependence below T_s, and a deviation from the B linearity becomes apparent at T well below T_s. A previous report showed this sublinear B dependence of Hall resistivity persists to 50 T,[23] which was ascribed to the B dependence of carrier density.

The B dependence of $\rho_{xy}(B)$ for annealed crystal is shown in Fig. 4(b). In stark contrast to the as-grown crystal, $\rho_{xy}(B)$ below T_s soon deviates from B linear dependence and exhibits nonmonotonic B dependence. Especially at $T = 5$ K, $\rho_{xy}(B)$ changes its sign to positive above $B \sim 4$ T. It is natural to attribute this B dependence of $\rho_{xy}(B)$ to the multiple-carrier effect. Intuitively, the negative sign of Hall coefficient at low field should be related to electrons with higher mobility, and the positive sign at high field indicates the prevalence of hole carriers with relatively lower mobility.

Obviously, the magnitude of residual resistivity, the B dependence of MR, and the nonmonotonic B dependence of ρ_{xy} are all correlated. They originate from the multiple-carrier contribution, which becomes clear as the sample quality is improved or as the carrier mobilities become higher. Below, in order to make more quantitative analysis on these results, we apply a multiple-carrier model to $\rho_{xy}(B)$.

E. Multiple-carrier model analysis

First, we used a simple two-carrier model fitting,[24] assuming one electron-type and one hole-type carrier. As is shown in the top panel of Fig. 5 (a), the two-carrier model fairly well fits $\rho_{xy}(B)$. However, the fitting parameter set shown in Table I seems not reasonable since (i) the density of holes is by two orders of magnitude larger than that of electrons, inconsistent with ARPES (Refs. 10–12) and quantum oscillation,[13,14] (ii) a

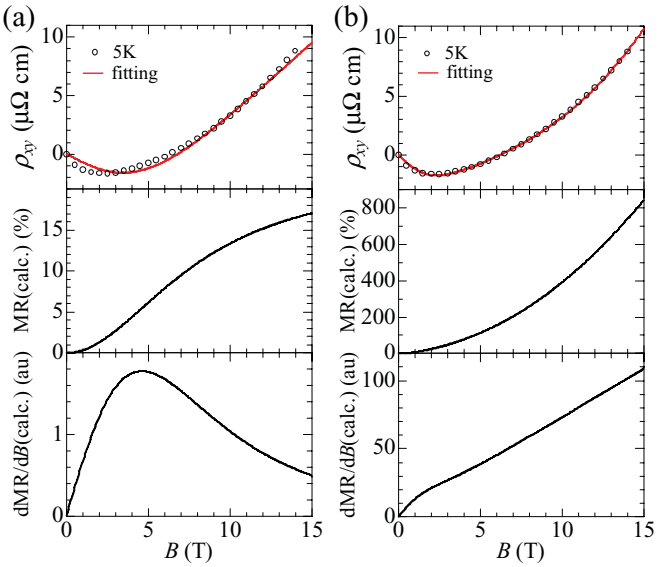

FIG. 5. (Color online) (Top panel) Fitting results for $\rho_{xy}(B)$ of annealed $BaFe_2As_2$ crystal in the magnetic field up to 14 T at $T = 5$ K using two-carrier (a) and three-carrier (b) models, respectively. (Middle panel) Calculated MR using the obtained parameter sets by fitting for $\rho_{xy}(B)$. (Bottom panel) Calculated $d\mathrm{MR}/dB$.

calculated MR using the obtained parameter set is ~15% at 14 T, much smaller than the experimental data [~800% at $B = 14$ T, see Fig. 6(b)], and (iii) the calculated MR shows saturating behavior, which can be seen as decrease of $d\mathrm{MR}/dB$ above 5 T [Fig. 5(c)]. Any other parameter sets do not lead to better fitting than that shown in Fig. 5(a) [in particular, if one put the constraint $n_e \sim n_h$, fitting of $\rho_{xy}(B)$ becomes worse]. Thus, the two-carrier model is insufficient to describe the B dependence of $\rho_{xy}(B)$ and MR.

In order to explain the experimental data, we add a third carrier instead of considering B-dependent carrier density and/or Dirac-cone states, namely, we apply three-carrier model fitting[24] (see the Appendix). One needs a number of parameters (carrier type, electron or hole, carrier density, and mobility for each carrier and their anisotropy) for three-carrier model fitting, but there are several constraints: (i) anisotropy would be negligible since the in-plane charge transport is almost isotropic, (ii) total carrier density should be of order of 10^{20} cm^{-3} as estimated from the Drude weight in the optical spectrum,[17] (iii) the densities of electrons and holes should be equal, as is also confirmed by the angle-resolved photoemission spectroscopy[10–12] and quantum oscillation data,[14] and

TABLE I. Values of parameters obtained by two- and three-carrier-model fitting to the Hall resistivity of annealed $BaFe_2As_2$ at $T = 5$ K in Figs. 5(a) and 5(b).

Carrier	1	2	3
Type	e (Dirac?)	e	h
n (two carrier) (10^{20} cm^{-3})	0.05(4)		6(2)
μ (two carrier) (10^3 cm^2/Vs)	1.5(3)		0.1(1)
n (three carrier) (10^{20} cm^{-3})	0.3(2)	0.7(2)	1.0(2)
μ (three carrier) (10^3 cm^2/Vs)	4.5(5)	1.5(2)	1.8(2)

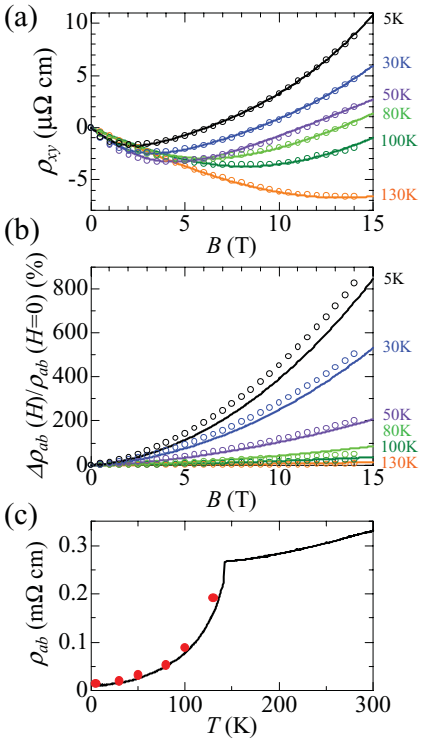

FIG. 6. (Color online) (a) Fitting results for $\rho_{xy}(B)$ of annealed $BaFe_2As_2$ crystal using the three-carrier model for various temperatures (solid lines). Open circles are experimental data. (b) Calculated MR using obtained parameter sets (solid lines). (c) Calculated in-plane resistivity (red dots). Black solid line is experimental data.

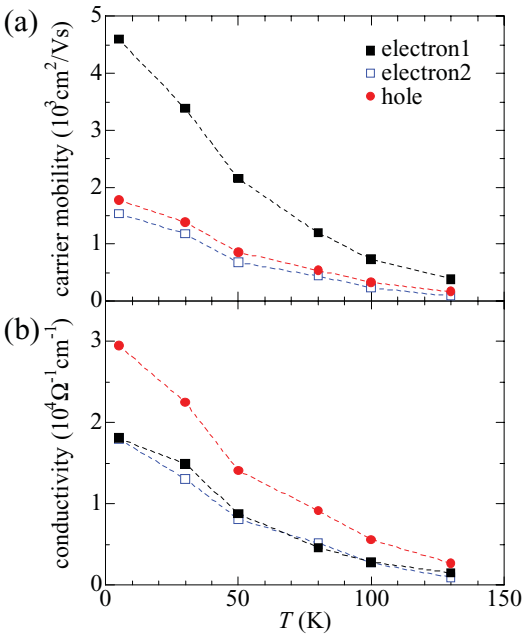

FIG. 7. (Color online) Temperature dependence of carrier mobility (a) and conductivity (b) obtained by the three-carrier model fitting.

(iv) the obtained parameter sets should be consistent with the magnitude of resistivity and MR.

In Fig. 5(b), we show the fitting results for $\rho_{xy}(B)$ at $T = 5$ K. The obtained parameter sets are shown in Table I. From the result of fitting, we find a few important points. First, $\rho_{xy}(B)$ of annealed crystal best fits when we assume one type of electron with very high mobility (μ_1^e) and smallest density (n_1^e), another type of electron with relatively low mobility (μ_2^e) and larger density (n_2^e), and holes with the largest density (n_3^h) and mobility comparable to the 2nd electrons (μ_3^h). Second, it is possible to reproduce the temperature dependence of $\rho_{xy}(B)$ by assuming reasonable temperature dependence of mobility for each carrier without changing the carrier density (Fig. 6). Third, $\rho_{xy}(B)$ of the as-grown crystal best fits by suppressing the mobility of each carrier using the same carrier density obtained from the fitting for $\rho_{xy}(B)$ of annealed crystal (see the Appendix). As is shown in Table I and Fig. 7, the three carriers each have distinct characters, but equally contribute to the charge transport.

F. Comparison with other experiments

One type of the electron carriers with highest mobility and smallest density that we extracted from the present results is likely to be associated with electron FS pockets originating from Dirac-cone-like energy bands with the Dirac point at ∼23 meV below E_F observed by ARPES measurements.[12] Note that there are two types of Dirac-type pockets with different sizes in $BaFe_2As_2$ as observed by ARPES,[12] and the Dirac-type pockets we consider here are larger ones, which are different from the tiny Dirac pockets, the dominant contribution to the charge transport of which has been discussed in previous reports.[7,8] As for the 2nd electron and the hole FS pockets we suppose, they are actually observed by ARPES.[10–12] The three types of carriers obtained in this study are in good agreement with the recent quantum oscillation measurement performed on annealed $BaFe_2As_2$ crystal.[14]

Since all the three carriers have high mobility as is shown in Table I (even the lowest one, $\mu_2^e = 1.5 \times 10^3$ cm^2/Vs at $T = 5$ K), together they probably form a narrow Drude component in the optical conductivity spectra,[15] which is in contrast to the previous reports suggesting the dominant role of tiny Dirac pockets.[7,8]

In fact, the B dependence of MR, especially the linear B dependence seen in the as-grown $BaFe_2As_2$ case, can not be explained even in the framework of the three-carrier model using the same parameter sets obtained by analyzing ρ_{xy}. In order to explain this behavior, we probably need to include the fourth carrier, which might be electrons with very small density (∼10^{17} cm^{-3}) and exclusively high mobility (∼10^4 cm^2/Vs), perhaps originating from tiny Dirac pockets. However, the contribution, if any, to the conductivity from such pockets has to be small in the annealed samples since the estimated conductivity (∼10^3 Ω^{-1}cm^{-1}) is much smaller than those of the three types of carriers we obtained in this study [Fig. 7(b)].

IV. CONCLUSIONS

We found that annealing $BaFe_2As_2$ crystals with BaAs is a very efficient way to improve the quality of the crystals. By using those annealed crystals, we observed strongly nonlinear B dependence of Hall resistivity and huge quadratic

B-dependent magnetoresistance at low temperatures in the magnetostructurally ordered state. In order to understand these transport properties, we applied the three-carrier model, two types of electrons and one type of hole, model analysis, and successfully reproduced the data quantitatively. These three types of carriers are in excellent agreement with recent quantum oscillation measurements made on similar high-quality crystals. All the three carriers are found to equally contribute to the conductivity. From the measurements on detwinned crystals, we found that the anisotropy of in-plane resistivity and its temperature range above T_s diminish as the sample quality is improved by annealing. This suggests that the so-far-conceived nematic phase is not intrinsic but induced by external pressure, impurities, or crystal disorder. Also, the in-plane resistivity is almost isotropic at temperatures well below T_s, even though the electronic state in the ordered phase is essentially anisotropic as evidenced by the optical conductivity. In the ordered state, a radical reconstruction of the FS takes place with gap opening in some part of the FS. Remaining carriers and reconstructed FS (two electron FS and one hole FS pocket) in the ordered state have isotropic contribution to the charge transport and mask the anisotropic charge dynamics at higher energies.

ACKNOWLEDGMENTS

We thank T. Terashima and N. Kurita for helpful discussions. S.I. and M.N. thank the Japan Society for the Promotion of Science (JSPS) for financial support. This work was supported by Transformative Research-Project on Iron Pnictides (TRIP) from the Japan Science and Technology Agency, and by the Japan-China-Korea A3 Foresight Program from JSPS, and a Grant-in-Aid of Scientific Research from the Ministry of Education, Culture, Sports, Science, and Technology in Japan.

APPENDIX

1. Fitting procedure

The fitting procedure is shown below. According to the three-carrier model,[25] the Hall resistivity is given by

$$\rho_{xy}(B) = \rho_{xx}(0)B(a + bB^2 + cB^4)/(1 + dB^2 + eB^4),$$

where

$$\rho_{xx}(0) = 1/\sum_i |en_i\mu_i|,$$

$$a = f_1\mu_1 + f_2\mu_2 + f_3\mu_3,$$

$$b = f_1\mu_1(\mu_2^2 + \mu_3^2) + f_2\mu_2(\mu_3^2 + \mu_1^2) + f_3\mu_3(\mu_1^2 + \mu_2^2),$$

$$c = (f_1\mu_2\mu_3 + f_2\mu_3\mu_1 + f_3\mu_1\mu_2)\mu_1\mu_2\mu_3,$$

$$d = (f_1\mu_2 + f_2\mu_1)^2 + (f_2\mu_3 + f_3\mu_2)^2 + (f_3\mu_1 + f_1\mu_3)^2 + 2(f_1f_2\mu_3^2 + f_2f_3\mu_1^2 + f_3f_1\mu_2^2)^2,$$

$$e = (f_1\mu_2\mu_3 + f_2\mu_3\mu_1 + f_3\mu_1\mu_2)^2,$$

$$f_i = |n_i\mu_i|/\sum_i |n_i\mu_i|.$$

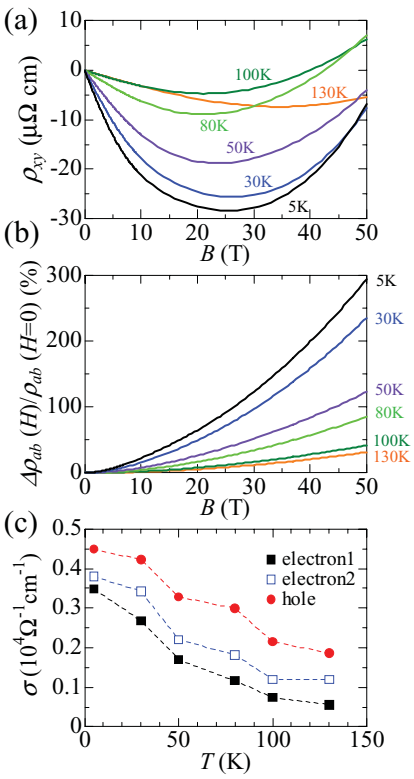

FIG. 8. (Color online) (a) Fitting results for $\rho_{xy}(B)$ of as-grown $BaFe_2As_2$ crystal in the magnetic field up to 50 T (Ref. 23) using the three-carrier model for various temperatures. Fitting parameters for $T = 5$ K data are shown in Table II. (b) Calculated MR. (c) Calculated conductivity σ.

Note that n_i and μ_i are the carrier density and mobility of the ith carrier, respectively, and the sign of the carrier mobility is negative for electrons and positive for holes in the calculation.

2. Three-carrier-model analysis of Hall resistivity of as-grown $BaFe_2As_2$ crystal

In Fig. 8(a), we show the results of three-carrier-model fitting for the Hall resistivity of as-grown $BaFe_2As_2$ crystal in the magnetic field up to 50 T.[23] Figure 8(b) shows the calculated MR using obtained parameter sets. We successfully reproduce those experimental data using the three-carrier model, without introducing the B dependence of carrier density. The mobility of each carrier is strongly suppressed compared with annealed $BaFe_2As_2$ crystal, but the carriers have almost equal contributions to the conductivity, as in the case of annealed crystal [Fig. 8(c)].

TABLE II. Values of parameters obtained by three-carrier-model fitting to the Hall resistivity of as-grown $BaFe_2As_2$ at $T = 5$ K in the magnetic field up to 50 T (Ref. 23).

Carrier	1	2	3
Type	e (Dirac?)	e	h
n (10^{20} cm^{-3})	0.2(2)	0.7(2)	1.2(2)
μ (10^3 cm^2/Vs)	1.1(3)	0.3(2)	0.2(2)

[1]M. Rotter, M. Tegel, D. Johrendt, I. Schellenberg, W. Hermes, and R. Pottgen, Phys. Rev. B **78**, 020503(R) (2008).
[2]Q. Huang, Y. Qiu, W. Bao, M. A. Green, J. W. Lynn, Y. C. Gasparovic, T. Wu, G. Wu, and X. H. Chen, Phys. Rev. Lett. **101**, 257003 (2008)
[3]J.-H. Chu, J. G. Analytis, K. De Greve, P. L. McMahon, Z. Islam, Y. Yamamoto, and I. R. Fisher, Science **329**, 824 (2010).
[4]M. A. Tanatar, E. C. Blomberg, A. Kreyssig, M. G. Kim, N. Ni, A. Thaler, S. L. Bud'ko, P. C. Canfield, A. I. Goldman, I. I. Mazin, and R. Prozorov, Phys. Rev. B **81**, 184508 (2010).
[5]E. C. Blomberg, M. A. Tanatar, A. Kreyssig, N. Ni, A. Thaler, Rongwei Hu, S. L. Bud'ko, P. C. Canfield, A. I. Goldman, and R. Prozorov, Phys. Rev. B **83**, 134505 (2011).
[6]R. Prozorov, M. A. Tanatar, N. Ni, A. Kreyssig, S. Nandi, S. L. Budko, A. I. Goldman, and P. C. Canfield, Phys. Rev. B **80**, 174517 (2009).
[7]K. K. Huynh, Y. Tanabe, and K. Tanigaki, Phys. Rev. Lett. **106**, 217004 (2011).
[8]H. H. Kuo, J.-H. Chu, S. C. Riggs, L. Yu, P. L. McMahon, K. De Greve, Y. Yamamoto, J. G. Analytis, and I. R. Fisher, Phys. Rev. B **84**, 054540 (2011).
[9]P. Richard, K. Nakayama, T. Sato, M. Neupane, Y.-M. Xu, J. H. Bowen, G. F. Chen, J. L. Luo, N. L. Wang, X. Dai, Z. Fang, H. Ding, and T. Takahashi, Phys. Rev. Lett. **104**, 137001 (2010).
[10]M. Yi, D. H. Lu, J.-H. Chu, J. G. Analytis, A. P. Sorini, A. F. Kemper, B. Moritz, S.-K. Mo, R. G. Moore, M. Hashimoto, W. S. Lee, Z. Hussain, T. P. Devereaux, I. R. Fisher, and Z.-X. Shen, Proc. Natl. Acad. Sci., USA **108**, 6878 (2011).
[11]M. Yi, D. H. Lu, J. G. Analytis, J.-H. Chu, S.-K. Mo, R.-H. He, M. Hashimoto, R. G. Moore, I. I. Mazin, D. J. Singh, Z. Hussain, I. R. Fisher, and Z.-X. Shen, Phys. Rev. B **80**, 174510 (2009).
[12]Y. K. Kim, H. Oh, C. Kim, D. Song, W. Jung, B. Kim, H. J. Choi, C. Kim, B. Lee, S. Khim, H. Kim, K. Kim, J. Hong, and Y. Kwon, Phys. Rev. B **83**, 064509 (2011).
[13]J. G. Analytis, R. D. McDonald, J.-H. Chu, S. C. Riggs, A. F. Bangura, C. Kucharczyk, M. Johannes, and I. R. Fisher, Phys. Rev. B **80**, 064507 (2009).
[14]T. Terashima, N. Kurita, M. Tomita, K. Kihou, C. H. Lee, Y. Tomioka, T. Ito, A. Iyo, H. Eisaki, T. Liang, M. Nakajima, S. Ishida, S. Uchida, H. Harima, and S. Uji, Phys. Rev. Lett. **107**, 176402 (2011).
[15]M. Nakajima, T. Liang, S. Ishida, Y. Tomioka, K. Kihou, C. H. Lee, A. Iyo, H. Eisaki, T. Kakeshita, T. Ito, and S. Uchida, Proc. Natl. Acad. Sci., USA **108**, 12238 (2011).
[16]C. R. Rotundu, B. Freelon, T. R. Forrest, S. D. Wilson, P. N. Valdivia, G. Pinuellas, A. Kim, J.-W. Kim, Z. Islam, E. Bourret-Courchesne, N. E. Phillips, and R. J. Birgeneau, Phys. Rev. B **82**, 144525 (2010).
[17]M. Nakajima, S. Ishida, K. Kihou, Y. Tomioka, T. Ito, Y. Yoshida, C. H. Lee, H. Kito, A. Iyo, H. Eisaki, K. M. Kojima, and S. Uchida, Phys. Rev. B **81**, 104528 (2010).
[18]T. Liang, M. Nakajima, K. Kihou, Y. Tomioka, T. Ito, C. H. Lee, H. Kito, A. Iyo, H. Eisaki, T. Kakeshita, and S. Uchida, J. Phys. Chem. Solids **72**, 418 (2011).
[19]H. C. Montgomery, J. Appl. Phys. **42**, 2971 (1971).
[20]C. Krellner, N. Caroca-Canales, A. Jesche, H. Rosner, A. Ormeci, and C. Geibel, Phys. Rev. B **78**, 100504(R) (2008).
[21]N. Ni, S. Nandi, A. Kreyssig, A. I. Goldman, E. D. Mun, S. L. Bud'ko, and P. C. Canfield, Phys. Rev. B **78**, 014523 (2008).
[22]A. A. Abrikosov, Phys. Rev. B **58**, 2788 (1998).
[23]H. Q. Yuan, L. Jiao, F. F. Balakirev, J. Singleton, C. Setty, J. P. Hu, T. Shang, L. J. Li, G. H. Cao, Z. A. Xu, B. Shen, and H. H. Wen, e-print arXiv:1102.5476.
[24]R. G. Chambers, Proc. Phys. Soc., London, Sect. A **65**, 903 (1952).
[25]J. S. Kim, J. Appl. Phys. **86**, 3187 (1999).